Quantifying multiple crystallite orientations and crystal heterogeneities in complex thin film materials

Journal:	*CrystEngComm*
Manuscript ID	CE-ART-06-2019-001010.R1
Article Type:	Paper
Date Submitted by the Author:	06-Aug-2019

Complete List of Authors:	Ogle, Jonathan; University of Utah, Chemistry Powell, Daniel; University of Utah, Chemistry Amerling, Eric; University of Utah, Chemistry Smilgies, Detlef; Cornell University, CHESS Whittaker-Brooks, Luisa; University of Utah, Chemistry

SCHOLARONE™
Manuscripts

ARTICLE

Quantifying multiple crystallite orientations and crystal heterogeneities in complex thin film materials

Received 00th January 20xx,
Accepted 00th January 20xx

DOI: 10.1039/x0xx00000x

Jonathan Ogle,[a] Daniel Powell,[a] Eric Amerling,[a] Detlef-M. Smilgies,[b] Luisa Whittaker-Brooks[a,*]

Thin film materials have become increasingly complex in morphological and structural design. When characterizing the structure of these films, a crucial field of study is the role that crystallite orientation plays in giving rise to unique electronic properties. It is therefore important to have a comparative tool for understanding differences in crystallite orientation within a thin film, and also the ability to compare the structural orientation between different thin films. Herein, we designed a new method dubbed the mosaicity factor (MF) to quantify crystallite orientation in thin films using grazing incidence wide-angle X-ray scattering (GIWAXS) patterns. This method for quantifying the orientation of thin films overcomes many limitations inherent in previous approaches such as noise sensitivity, the ability to compare orientation distributions along different axes, and the ability to quantify multiple crystallite orientations observed within the same Miller index. Following the presentation of MF, we proceed to discussing case studies to show the efficacy and range of application available for the use of MF. These studies show how using the MF approach yields quantitative orientation information for various materials assembled on a substrate.

KEYWORDS (mosaicity factor, multiple crystallite orientations, GIWAXS)

Introduction

Thin film technologies continue to dominate a multiplicity of materials science research fields and are rapidly dominating the electronics and photovoltaics markets. Current state-of-the-art thin film technologies seek to develop a deeper understanding of the complex interplay between processing conditions, electronic structure, and morphology. A suite of diffraction and spectroscopic tools has been developed to probe this important interplay as it has a strong bearing on the practical properties of a material. Of these tools, X-ray diffraction-based analysis techniques such as X-ray powder diffraction, X-ray crystallography, and grazing incidence X-ray diffraction continue to play an integral role within the material characterization framework. In both single-crystal and polycrystalline materials, X-ray diffraction measurements are essential characterization techniques for investigating lattice strain parameters, lattice constants, relaxation, crystallinity, material composition, phase identification, crystallite size, and orientation in thin film materials.[1] Within the family of X-ray diffraction characterization techniques, grazing incidence wide-angle X-ray scattering (GIWAXS) is often used to qualitatively and quantitatively determine the orientation distribution function (ODF) of thin films.[2–7] Understanding and controlling the various parameters (e.g., growth mechanism, intrinsic crystal size and texture, processing conditions, and sample-substrate interactions) that cause a crystallite within a material to orient in a particular fashion when cast as a thin film are of paramount importance for predicting and tailoring material properties as specific orientations can yield desired electrical properties.

The ODF of a material plays a critical role in the overall performance of polycrystalline and semi-crystalline materials. This is especially true for both organic and organo-metal semiconducting materials where their structure and morphology directly affect their electrical properties.[8–12] Due to device geometry constraints, thin film transistors, for example, necessitate materials with large lateral electron mobilities; therefore, the thin film materials used for this particular application require a high degree of preferential crystallite orientation aligned parallel to the substrate (edge-on orientation).[13,14] Conversely, thin film diodes and solar cells should be assembled with materials having large electron mobility values in the vertical direction; thus crystallites within the thin film must be oriented “face-on” with respect to the substrate.[15–17] Depending on the application, researchers may study the impact of processing methods on the preferential orientation of a crystallite within a material using GIWAXS.[2,4,11,18] When accounting for all other factors impacting charge transport (i.e., crystallite size and crystal structure), anisotropic charge transport properties observed in thin films may be compared directly to the orientation of a material by measuring the distribution of orientation for a given reflection. GIWAXS studies may be used to understand the ODF of a material. Fig. 1 shows an experimental setup for collecting a GIWAXS pattern with the respective q_z and q_{xy} coordinates

[a] Department of Chemistry, University of Utah, 315 South 1400 East, Salt Lake City, Utah, 84112, USA
[b] Cornell High Energy Synchrotron Source, CHESS, Cornell University, Ithaca, NY, 14853

Electronic Supplementary Information (ESI) available: [details of any supplementary information available should be included here]. See DOI: 10.1039/x0xx00000x

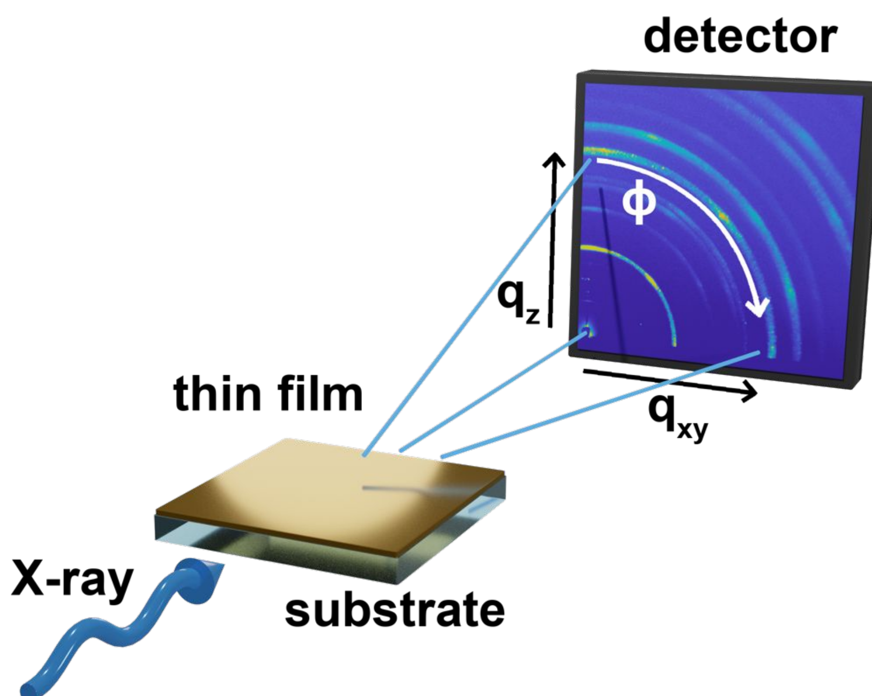

Fig. 1 GIWAXS experimental setup with q_z and q_{xy} coordinates and φ labeled on the GIWAXS pattern. q_z denotes scattering observed out-of-plane with respect to the substrate, q_{xy} denotes scattering observed in the plane of the substrate, and φ denotes the scattering observed along a specific q.

along each axis as well as an integrated azimuthal trace highlighted across the angle φ (phi) for a specific (hkl) reflection. Scattering along a two-dimensional detector system is measured in reciprocal space where q_z is scattering signal along the z-axis and q_{xy} accounts for any signal along the xy plane of the film. The angle φ, along which the orientation of a Miller index reflection is observed, is then defined as the angle relative to the beam center sweeping from the azimuth down to the plane of the film in degrees from 0° to 90°.

Quantifying the crystallite orientation in thin film materials via GIWAXS is typically performed using the Hermans' orientation function (HF).[15,19–23] In 1946, Hermans et al. published a seminal work in which they developed a mathematical relationship to describe the degree of crystallite orientation in vertically aligned cellulose spindle fibers held normal to an incident X-ray beam.[24] The orientation factor, HF, that they proposed to measure crystallite orientation is designed from mathematical constructs formulated from the ideal chain polymer model which treats polymeric monomers as non-interacting subunits.[24–27] A reflection for a specific (hkl) Miller index is observed by measuring the scattered X-ray intensity as a function of orientation. Despite the initial niche application of HF for investigating structural and morphological characteristics of cellulose fibers, the value of this method in quantifying the degree of preferential orientation within other samples was later recognized with the development of GIWAXS. HF has since become a commonly applied method for quantifying the orientation of a crystallite related to a particular set of Miller index reflections, (hkl), in thin film materials, particularly in organic electronics. HF is defined as:

$$HF_{hkl} = \frac{3\langle\cos^2\varphi_{hkl}\rangle - 1}{2} \tag{2}$$

This is a 2nd order Legendre polynomial of $\langle\cos^2\varphi_{hkl}\rangle$, which can be defined as:

$$\langle\cos^2\varphi_{hkl}\rangle = \frac{\int_0^{\pi/2} I(\varphi)\sin\varphi\cos^2\varphi\, d\varphi}{\int_0^{\pi/2} I(\varphi)\sin\varphi\, d\varphi} \tag{3}$$

Where φ is the azimuthal angle relative to the incident X-ray beam and I(φ) is the intensity of the (hkl) reflection along φ. HF determines the orientation of a crystallite having a specific Miller index reflection by fitting equations 2 and 3 to the intensity distribution along φ relative to the thin film substrate, where φ = 0° is normal to the substrate. Values of HF range from 1 to -0.5. If all the signal intensity for a given Miller index reflection is observed exclusively out-of-plane with respect to the substrate (φ = 0°) HF will yield a value of 1. If all of the signal intensity is in-plane with respect to the substrate (φ = 90°), HF will be equal to -0.5. If the intensity is equivalent at all angles, HF will have a value of zero corresponding to a completely isotropic ODF. Based on the mathematical constructs,[24] HF assumes that the orientation of the crystallites in a given material fit a single Gaussian distribution (PG) which can be described in terms of the mean (μ) and the standard deviation (σ) in the form:

$$P_G(x) = \frac{1}{\sqrt{2\pi}\sigma} e^{-\frac{(x-\mu)^2}{2\sigma^2}} \tag{1}$$

This journal is © The Royal Society of Chemistry 20xx

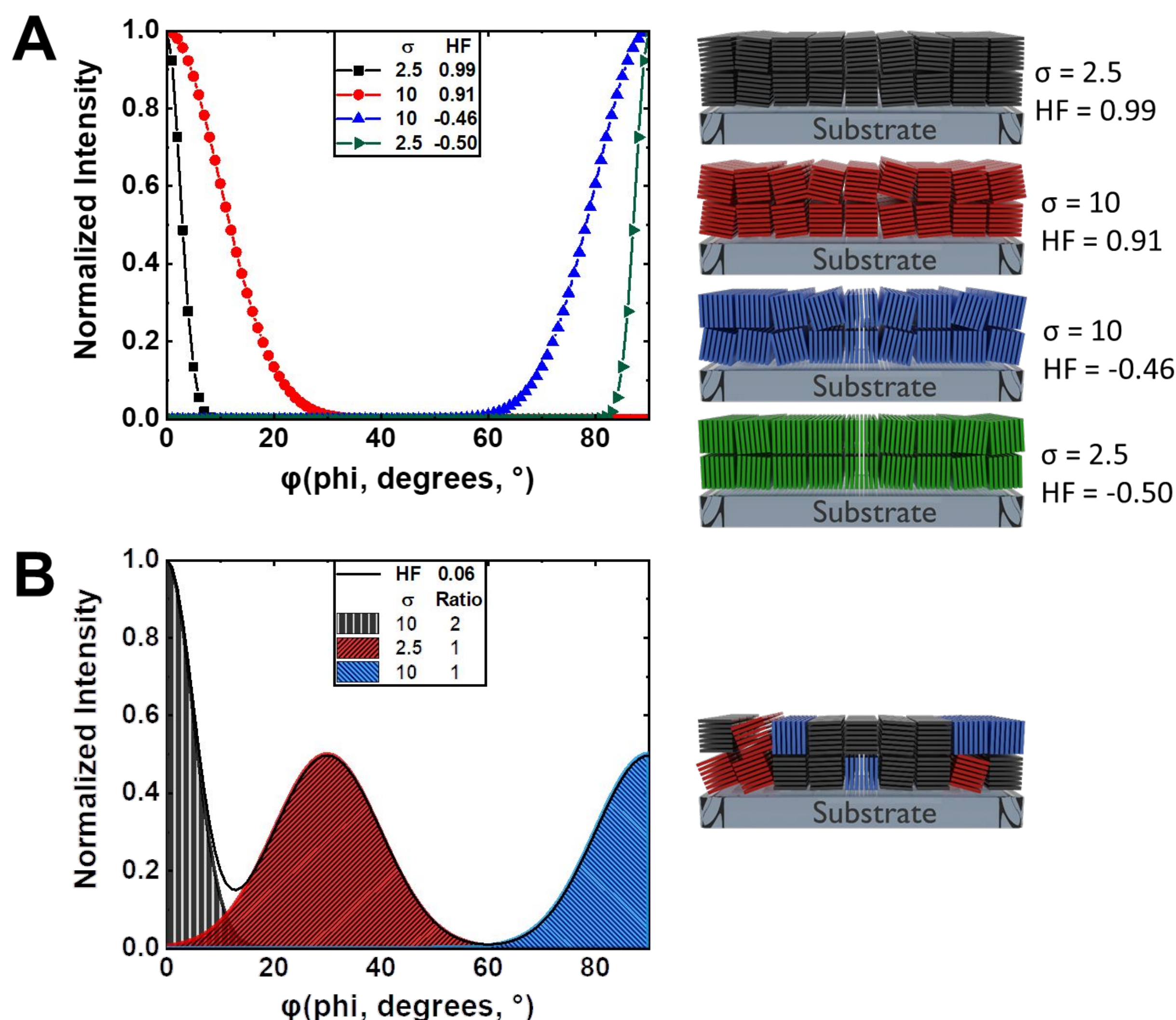

Fig. 2 Limitations of the HF method that arise when favorable orientations are present at more than one angle. (A) Comparison of different Gaussian distributions of varying width centered at both φ = 0º and φ = 90º, and an accompanying animation depicting their respective crystallite orientations shown to the right. (B) The combination of three different crystallite orientations within a single film atop a substrate, and an animation of the crystallite orientations.

Where x is the location along φ and μ describes the mean value of the Gaussian which, in the case of GIWAXS, is the angle relative to the substrate at which the maximum is observed. The standard deviation σ of the Gaussian distribution then determines how well oriented the sample is; the wider this distribution, the less oriented the sample. Therefore, HF can be used as a quantitative description of sample orientation and is a powerful comparative tool that has been used to better understand the relationship between processing conditions, electronic characteristics, chemical structure, morphology, and orientation in thin film materials.

As the structural information in thin film materials has become more complex due to the interplay between multiple crystallite orientations, as well as contributions arising from amorphous regions, our ability to discern and quantify orientation using HF has stagnated due to several intrinsic limitations with the method. The following will discuss four chief limitations encountered when using HF as an analytical tool to determine crystallite orientation in thin film materials.

The first limitation arises from the numerical design of HF, where orientation normal to the substrate is valued at a scale of 1 and the parallel orientation is valued at a scale of -0.5. As the shape of the HF function is not symmetric about φ = 45, there is no feasible mechanism to directly compare these HF values nor determine whether the differences observed in orientation affect the electrical properties of the film. This constraint is illustrated in Fig. 2A, which depicts four different simulated azimuthal traces of an (hkl) reflection for a thin film material. The example shows two different standard deviations (σ = 2.5 and σ = 10), each placed along the normal and parallel directions with measured values of $HF_{\sigma=2.5} = 0.99$ and $HF_{\sigma=10} = 0.91$ normal to the substrate, and $HF_{\sigma=2.5} = -0.50$ and $HF_{\sigma=10} = -0.46$ parallel to the substrate. Since these values are on different scales, the orientation along the normal axis cannot

be directly compared to the orientation along the parallel axis. As such, HF cannot be used to quantify differences in orientation between films oriented along different axes.

The second limitation is observed as a consequence of the first limitation—thin film materials having crystallites that exhibit multiple favorable orientations cannot be directly compared. For example, Fig. 2B shows the intensity distribution as a function of φ for a thin film material with different crystallite orientations along a single (hkl) reflection. HF in this example is measured to be 0.06 implying no orientation, which does not match the three orientation distributions presented in Fig. 2B. Moving beyond the initial constraint encountered when comparing reflections oriented along the normal and parallel axes as stated above, analysis of ODF in thin film materials having crystallites with multiple favorable modes of orientation between these axes may not be evaluated.

Another major limitation can be encountered when HF is calculated for an (hkl) reflection whose intensity along φ is comprised of more than one Gaussian distribution width oriented in the same direction (which in practical terms would correspond to different crystallite orientations along φ in a thin film). Fig. 3A shows various calculated I vs. φ plots. Four are single Gaussian signals with increasing standard deviations of σ = 1, 3, 15, and 24 all oriented along the primary axis, φ = 0°. As the standard deviation of each respective Gaussian signal increases, HF decreases from HF(σ=1) = 1.00, HF(σ=3) = 0.99, HF(σ=15) = 0.82, and the widest distribution down to HF(σ=24) = 0.60. The final signal is composed of two Gaussians with standard deviations of σ = 1 and σ = 24 weighted at 95% and 5%, respectively. While qualitatively the double Gaussian appears to be mostly comprised of σ = 1, quantification using HF(σ=1, σ=24) reports that the orientation is comparable to the least oriented signal σ = 24. This phenomenon arises from an inherent weakness in the design of HF; it is only capable of appraising the orientation of systems exhibiting a single Gaussian intensity distribution. As the mathematical design of HF is not intended for multiple-Gaussian systems, the convolution of σ = 1 and σ = 24 yields errant orientation values. This limitation can be overcome by fitting the individual components of multiple Gaussian systems, but limitations in the ability to discern when and where multiple Gaussians should be fit to an intensity makes it difficult to accurately determine the HF value for a given orientation distribution within a thin film comprising crystals with multiple orientations.

A final limitation can be observed when HF is calculated for data sets where a small contribution of noise will significantly affect the measured orientation. As demonstrated in Fig. 3B, a single Gaussian of σ = 2.5 with less than 1% random noise returns an HF of 0.23, while an equivalent Gaussian which has no noise yields an HF of 0.99. The significant deviation in orientation values between samples with and without artificial noise illustrates how very small variations in the signal can drastically alter HF values. Issues with noise are often mitigated in practice by eliminating it in areas where the user is confident that there is no scattering signal. This is done by taking the average intensity and applying the obtained value to the regions where no scattering signal is observed. This technique typically

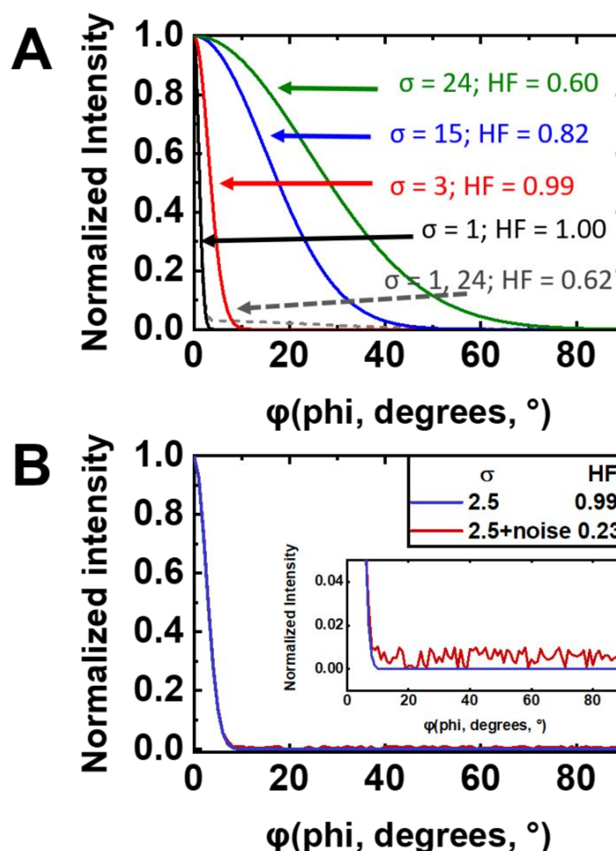

Fig. 3 Issues observed when using HF. (A) A comparison of Gaussian distributions centered at φ = 0º with increasing standard deviations and respectively decreasing HF values. A convolution of two Gaussian distributions (σ = 1, 24) is also shown. (The HF value for the combined Gaussians erroneously implies a relatively non-oriented sample). (B) A Gaussian signal with and without the presence of <1% noise.

yields an HF value that more closely approaches its true value. However, it is not always possible to mitigate issues that arise from noise; for example, when the intensity significantly changes along φ, the procedure as mentioned above may not be used. The issue of noise and multiple Gaussian distributions can render calculated HF values as potentially arbitrary.

We have demonstrated that a number of limitations and critical issues may arise when using HF to determine crystallite orientation. The inability to directly compare HF values within samples having crystallites exhibiting multiple orientations and the inability to use it to characterize orientations that occur along a non-primary axis of interest is axiomatic. As the morphology and structural order in crystalline thin film materials begin to conform to more complex ODF motifs that HF is not capable of properly characterizing, the need for a methodology to accurately quantify their crystallite orientation also becomes very necessary. With these challenges in mind, we report a new method dubbed the mosaicity factor (MF) for quantifying crystallite orientation in thin films using GIWAXS scattering patterns. MF overcomes all of the limitations previously outlined and is capable of characterizing the

This journal is © The Royal Society of Chemistry 20xx

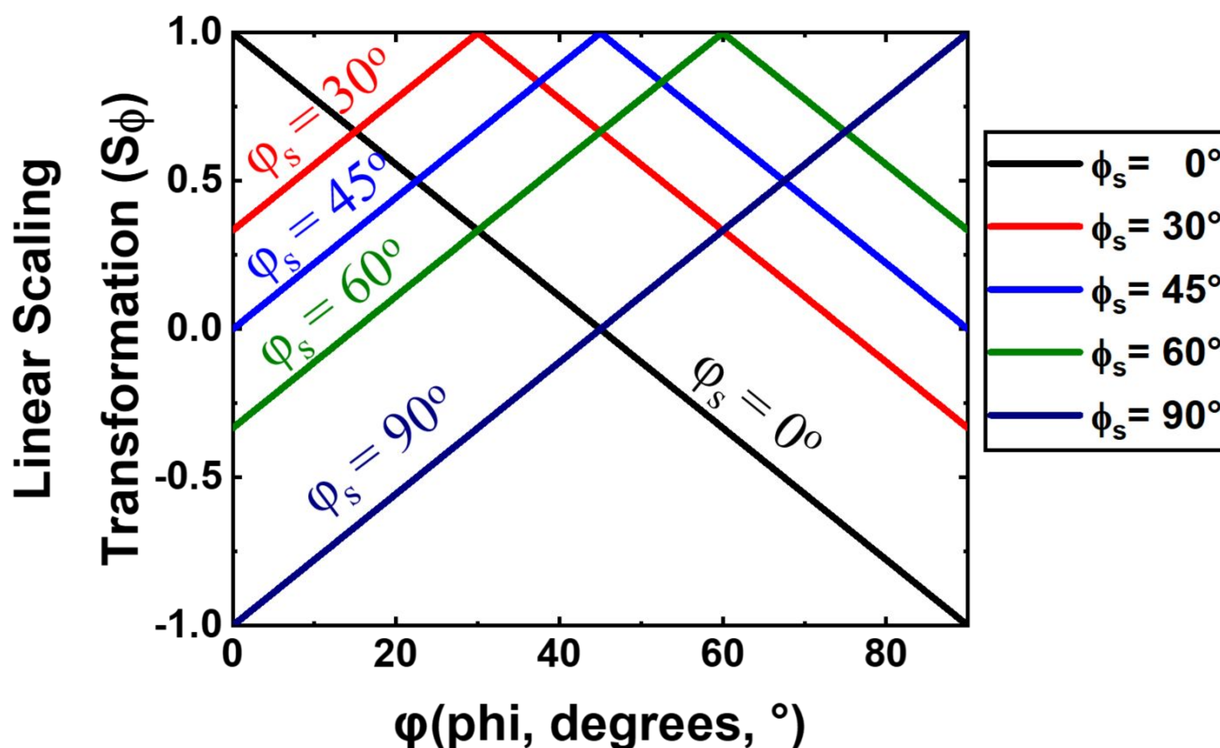

Fig. 4 Linear scaling transform values for quantifying the orientation of a crystallite centered along φ_s. Note that the absolute value of the slope in each transform is equivalent when moving away from φ_s.

orientation of multiple signal peaks within a given azimuthal trace. For the sake of comparison, computed HF and MF values will both be presented in our examples.

Proposed method

The MF method uses a common GIWAXS coordinate system as shown in Fig. 1, where it is assumed that the xy plane is parallel to the surface of the substrate. GIWAXS scattering patterns for thin films collected at a Synchrotron source must first be corrected for the horizontally polarized synchrotron radiation source as well as any background contribution from the substrate. This has been thoroughly reported, and it is an integral part of most software packages designed to compute and analyze GIWAXS data collected for thin films.[3,28,29] MF is designed to quantify the ODF of multiple observed orientations within a sample or compare ODF changes between different thin films. When there is only one observed orientation within a thin film, MF can be used “as is” to study the orientation over a range of 0° to 90°. If multiple orientations are observed, MF can be applied to the separate components of the azimuthal trace. If there are non-oriented crystallites present in the sample (isotropic signal), there will be equivalent observed scattering intensity at all φ. Once the non-oriented sample has been accounted for, individual favorable orientations can be quantified by characterizing each respective signal over a given φ range that each signal is present over. Finally, if the change in φ along the azimuthal trace is equidistant, then the percentage contribution can be attained through numerical integration of each discrete component. In this way, a film can be characterized for the orientation of each respective component (i.e., oriented and non-oriented crystallites) and the percent contribution to the total ODF.

Linear scaling transformation

In order to assess orientation along I(φ), an evaluative coordinate system capable of comparing how a signal is oriented along q_z vs. q_{xy} must be established. This can be accomplished by transforming respective φ values to a scale of 1 to -1 for φ angles from 0° to 90°, as shown in equation 4:

$$S(\varphi) = \frac{45-\varphi}{45} \quad (4)$$

where, S is a linear scaling transformation of φ. This relationship implies that all signal oriented at 0° is perfectly oriented along the q_z and corresponds to a value of 1, while signal oriented along the q_{xy} is defined as diametrically oriented to the q_z and is valued as -1. Signal observed at 45° can be understood as a signal that is 50% oriented along the q_z and 50% oriented along the q_{xy} and is equal to 0.

Equation 4 can be further modified to allow for the evaluation of a signal corresponding to orientation along any desired angle. This is accomplished by shifting S_φ to the desired angle (φ_s) as shown in equation 5:

$$S_{\varphi_s}(\varphi) = \frac{45-|\varphi_s-\varphi|}{45} \quad (5)$$

This linear transform will then allow for the orientation to be characterized centered at φ_s, and would decrease linearly along the same scale as per equation 4 when the angle deviates from

φ_s as shown in Fig. 4. This allows for a signal that is centered along different angles to be weighted directly according to how close to the angle of interest the signal is observed. In this manner, the orientation along any non-primary axis may be calculated and will allow for the orientation distribution along any axis to be compared between samples. This can then be coupled with a weighted amplitude to quantify the orientation.

Weighted amplitude

The amplitude being quantified must be weighted in order to normalize the signal in a manner that will allow for the measured amplitude to be consistent between samples. The weighted amplitude (A_w) at each point along a specified range of angles is defined as:

$$A_w(\varphi) = \frac{A(\varphi)}{\Sigma A} \quad (6)$$

Where A_w is the amplitude at a given φ divided by the sum of the amplitudes over the area within the φ characterization window. When computing the orientation of a scattering signal observed from 0° to 20°, for example, the amplitude is weighted using only the values from that explicit range between 0° and 20°. A caveat to determining the weighted amplitude deals with how to properly give weights to the starting and ending amplitudes, which is given by:

$$A_{\varphi=0°,90°} = 0.5 \times A_{\varphi=0°,90°} \quad (7)$$

As per equation 7, any intensity observed at 0° or 90° only contributes half of its intensity within the constraints of comparing intensity between the respective angles. Thus, any intensity value observed at exactly 0° or 90° must be corrected so that its contribution is half of its intensity. This issue is further discussed in the supporting information. Fig. 5A depicts visual examples of simulated sample intensity signals which are converted to their respective weighted amplitudes as shown in Fig. 5B. Note that in these examples the amplitude values at 0° are divided in half to account for the overlap contribution. These examples also show that Aw can and should be calculated over specific areas of interest. If the orientation of an (hkl) reflection is only observed within a certain range and needs to be quantified, then the weighted amplitude should be computed exclusively within this specified range. In this way, if there are different (hkl) reflection intensities observed within a thin film, the orientation for each reflection and hence the orientation of a particular crystallite may be measured as a function of its signal.

Mosaicity factor (MF)

By using the angular transformation (equation 5) and the weighted amplitude coefficient at each data point (equation 6), the orientation of a given (hkl) reflection may be computed by the product sum of each component, and has been dubbed the mosaicity factor, MF, given by equation 8:

$$MF_{(hkl);\varphi_s}(\varphi) = \Sigma A_w(\varphi) S_\varphi(\varphi) = \Sigma \frac{A(\varphi)}{\Sigma A}\left[\frac{45 - |\varphi_s - \varphi|}{45}\right] \quad (8)$$

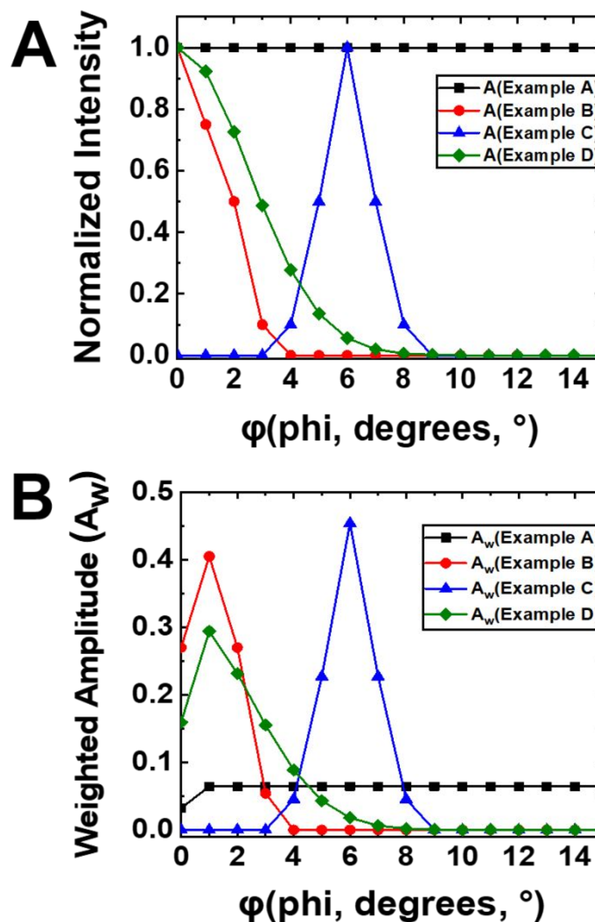

Fig. 5 Conversion of four example distributions (A) into their respective weighted amplitudes (B), including the value at φ = 0º being half of the normal intensity.

MF values offer two unique comparative modes to users. First, determining an MF value for a reflection with a specific Miller index enables the user to infer the overall crystallite orientation along any direction of a material within a thin film and even compare changes in orientation between different thin films as a result of a controlled variable of interest (e.g., processing conditions). Second, MF values may be used to compare differences in multiple observed crystallite orientations within a single sample. In this case, MF may be used to analyze the percent contribution of a given peak to the overall orientation of a sample. This evaluation can be used to compare differences in orientation within a single film wherein a reflection may have a different MF along 0° when compared to 90° or some other angle. In this sense, crystallites having different orientations (or no orientation) may be easily compared.

Case studies: utilizing MF to determine crystallite orientation in technologically relevant thin film materials

All GIWAXS data used herein for testing the MF method were obtained at the D1 and G1 stations of the Cornell High Energy Synchrotron Source (CHESS). To limit issues with geometric

This journal is © The Royal Society of Chemistry 20xx

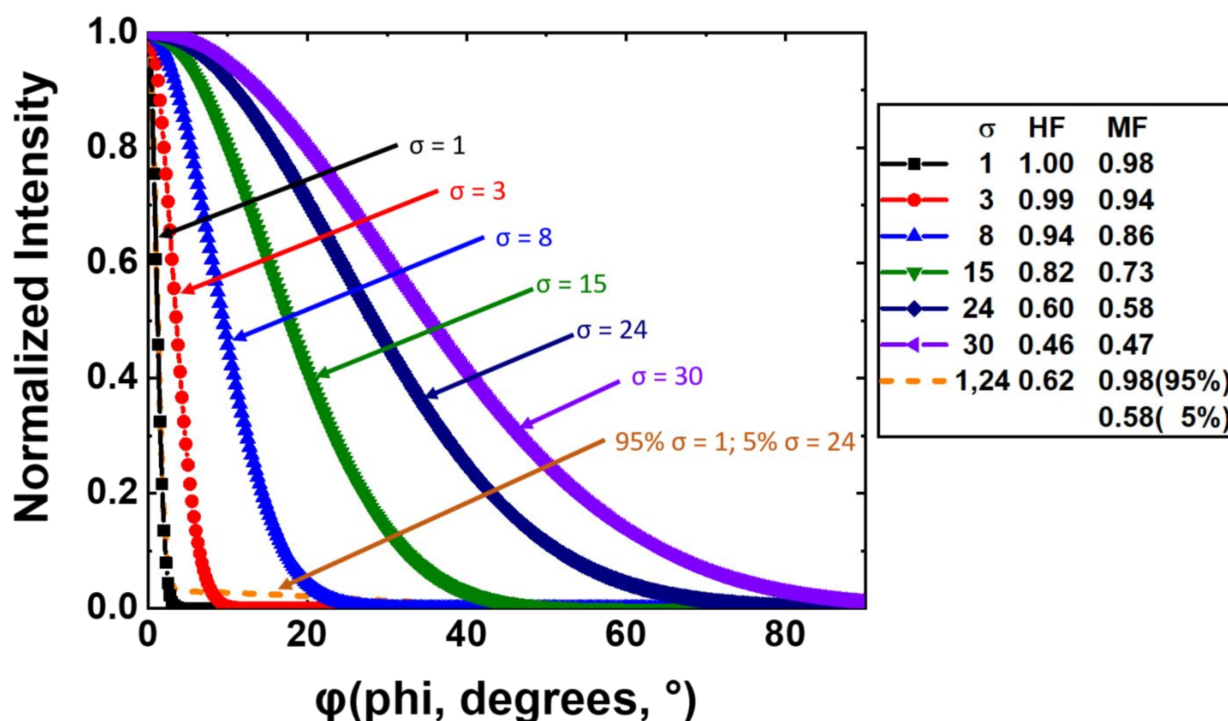

Fig. 6 Gaussian distributions centered at φ = 0° with increasing standard deviations, as well as the combination of two Gaussian distributions (95% σ = 1 and 5% σ = 24). Their respective HF and MF values are also listed for clarity.

smearing of the peaks on the detector, the width of samples in the direction of the beam was kept to 0.5 cm.[30–32] As each sample was collected on different dates, sample specific conditions are listed in the supporting information. All GIWAXS images and linecuts were processed using the graphical user interface GIXSGUI.[28] The MF and HF for each sample were then computed using the MATLAB code ShekieFactor.m. ShekieFactor.m requires one input ASCII text file comprised of I vs. φ data ranging from 0° to 90° in a tab-delimited format. This code allows for an efficient method to determine and compare both MF and HF for the entire azimuthal trace and can calculate crystallite orientation based on specific reflections as well as the degree of non-oriented crystallites. Users interested in a purely practical approach for determining the crystallite orientation factor in novel thin film materials using MF may download the MATLAB code ShekieFactor.m from the supporting information section. We also recommend using the MF analytical tool in conjunction with scanning electron and/or transmission electron microscopy studies since these techniques may provide corroborating features about the morphology and local orientation of crystallites within a thin film.

Gaussian distributions

Fig. 6 illustrates the main differences between MF and HF, wherein a set of Gaussian peaks with various widths: σ = 1; σ = 3; σ = 8; σ = 15; σ = 24; and σ = 30 are evaluated using both methods. At both the narrow and wide extremes of the Gaussian distributions (σ = 1 and σ = 30), MF and HF report very similar values. However, as σ transitions from 3 down to 24, the increasing distribution of the Gaussian signal returns values for MF and HF that begin to differ. The values shown in Fig. 6 indicate that MF is more sensitive when quantifying the orientation of preferentially aligned crystallites with Gaussian distributions of σ ranging from 1 to 15. Conversely, HF is more of a useful analytical approach when quantifying the orientation of less oriented crystallites with Gaussian distributions of σ ranging from 15 to 30. It can be inferred that, because the structural orientation quantified using HF and MF yield different values and their sensitivity to change is different, they cannot be directly compared with one another. We can also represent two Gaussian distributions weighed at 95% σ = 1, and 5% σ = 24. As such, crystallites having a distribution fingerprint comparable to these two Gaussians can be studied in two different ways using MF, the more informative being the deconvolution and analysis of the underlying Gaussian signals, and the slightly less informative being the overall orientation of the combined systems. The more informative method for these two combined Gaussians yields the respective MF values of the underlying Gaussian signals with the respective intensities of each observed signal. This method can be used to infer that 95% of crystallites with a given (hkl) Miller index within the thin film show an $MF_{(hkl);0^\circ} = 0.98$, while 5% of the crystallites in the film exhibit a less oriented $MF_{(hkl);0^\circ} = 0.58$. The overall orientation of these two Gaussian signals returns an $MF_{(hkl);0^\circ} = 0.81$ which, when directly compared to HF, shows an increase of 0.19 in orientation but as we established with the varying Gaussian distribution widths going from σ =1 to σ =30, MF and HF cannot be directly compared to one another. In order to directly compare these values, a single Gaussian with $MF_{(hkl);0^\circ} = 0.81$ can be measured for HF orientation which yields a value of HF = 0.90, showing that the MF measured for this example implies that crystallites within a thin film would be

mostly oriented normal to the substrate. Both of these measurements can be used to better understand the orientation of multiple crystallites within a thin film.

Quantifying orientation along various angles

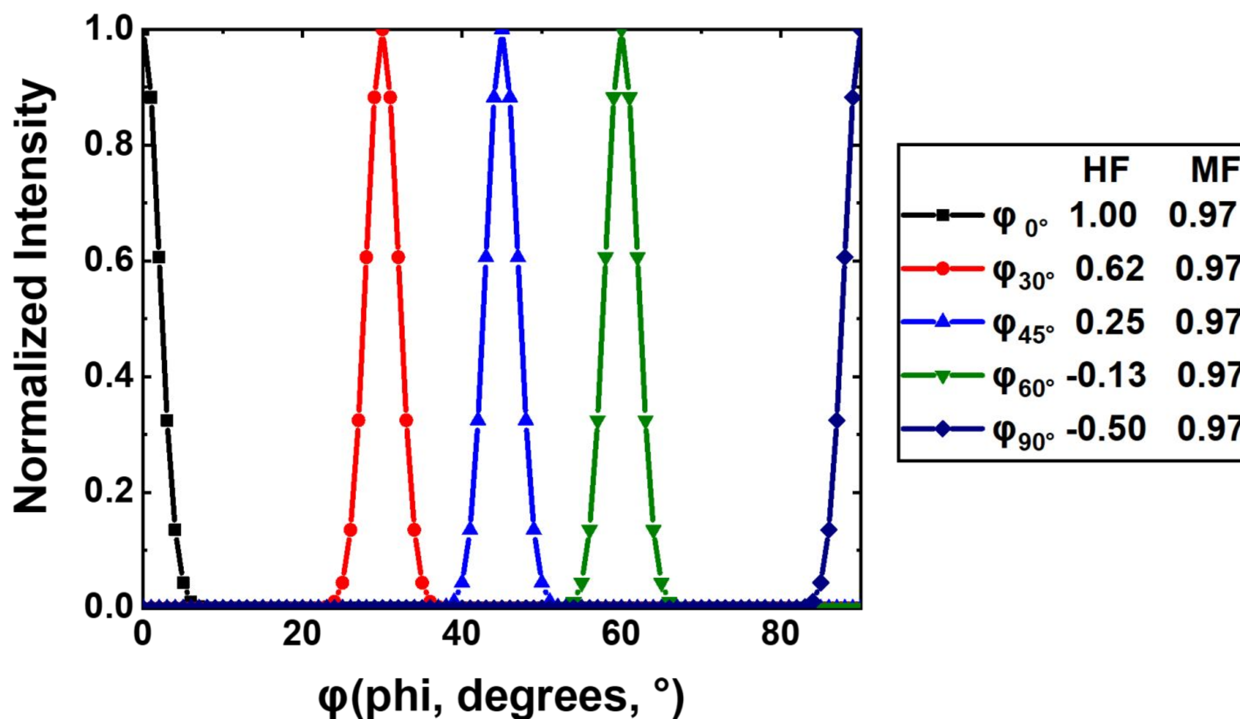

Fig. 7 Comparison of Gaussian distributions oriented along different angles φ_s with respective HF and MF values listed in the legend.

MF uniquely enables users to directly compare computed orientation values along different axes of interest as illustrated in Fig. 7, where five Gaussians of equal distribution width (σ = 2) along various angles are shown. As depicted, reflections that are localized at any angle can be quantified for orientation and compared with one another. Here, all reflections return the same $MF_{(hkl);0°} = 0.97$ along each respective angle. This shows that MF can be used to directly compare the orientation of crystallites along different angles.

Case studies

Simulated scattering data sets with different Gaussian distributions have been used to overview the strengths and capabilities of MF. To follow this, experimentally obtained GIWAXS patterns of thin films comprising either inorganic, organic, or organic-inorganic hybrid materials will be used to determine their crystallite orientation using MF. Furthermore, the GIWAXS patterns for these very different thin film materials will allow us to show the capability of the MF method to characterize crystallite orientation at various distributions when signal noise is present, and that our MF method may be used to study thin film materials over a large breadth of applications.

Organic-inorganic hybrid perovskite thin films. Organic-inorganic hybrid perovskites (OIHPs) have gathered considerable attention within the semiconductor community due to their unique photophysical and electronic properties, such as high absorption coefficient, tunable excitonic properties, low trap-state density, and long carrier diffusion lengths (1-2 μm) and carrier lifetimes.[33–37] These properties, coupled with their solution processability, have poised OIHPs as potential materials not only for photovoltaics but also in device applications spanning from light-emitting diodes, photodetectors, and field-effect transistors.[38–40] However, the low enthalpy of formation of OIHPs acts as both a blessing and a curse when it comes to advantageous thin film preparation protocols and unfavorable degradation in the presence of oxygen and moisture, respectively.[41–45] It is well documented that the instability of OIHPs towards oxygen and moisture may be improved by reducing their dimensionality from the well-studied three-dimensional system to a two-dimensional OIHP system. Ruddlesden-Popper phase perovskites are two-dimensional OIHPs that follow the generic formula $A'_2A_{n-1}B_nX_{3n+1}$ (A' = bulky organic cation spacer; A = small organic or inorganic cation; B = Pb^{2+}, Ge^{2+}, or Sn^{2+}; X = Cl^-, Br^-, I^-; n is an integer). Ruddlesden-Popper OIHPs are composed of self-organized building blocks where sheets of corner-shared $[BX_6]^{4-}$ octahedra are stacked along the c-axis, separated by large organic cation spacers on either side of the inorganic octahedra (Fig. 8A). The anisotropic structure of the Ruddlesden-Popper OIHPs has a large impact on their in-plane vs. out-of-plane charge transport characteristics.[36,46] The structural orientation of 2D Ruddlesden-Popper OIHPs, with respect to the substrate and upon different processing conditions, will significantly affect their electronic properties.[47] Fig. 8B shows a scanning

 This journal is © The Royal Society of Chemistry 20xx

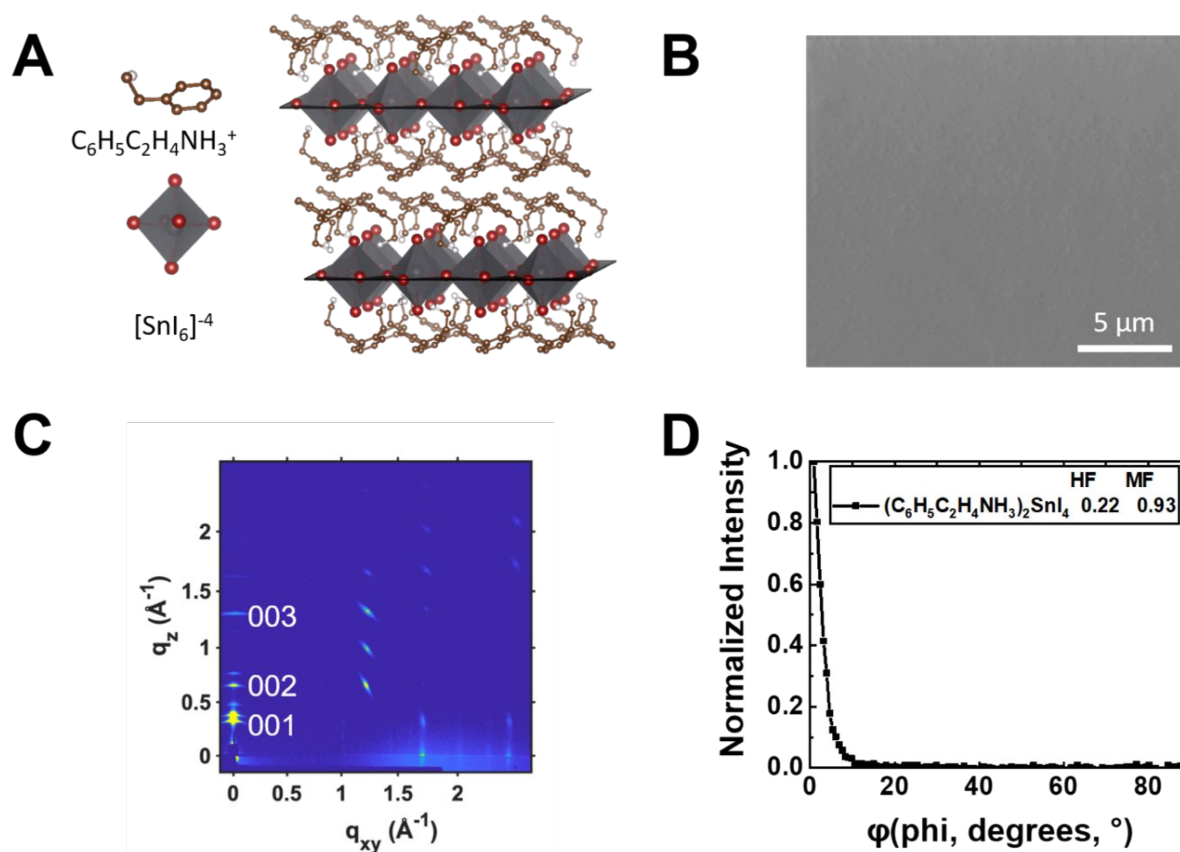

Fig. 8 Case study: phenethylammonium tin iodide. (A) 3D representation of the phenethylammonium tin iodide structure comprised of tin iodide sheets separated by phenethylammonium layers. (B) Scanning electron micrograph of a phenethylammonium tin iodide thin film showing a very uniform morphology. (C) GIWAXS pattern of a phenethylammonium tin iodide thin film showing structural orientation with the (00l) indices reflecting along the out-of-plane direction. (D) Normalized intensity of the (002) reflection plotted as a function of φ, the azimuthal angle measured from $q_{xy} = 0$. HF and MF values are also listed.

electron micrograph for a 2D phenethylammonium tin iodide - $(C_6H_5C_2H_4NH_3)_2SnI_4$ (also represented as $(PhEA)_2SnI_4$) thin film. These films were prepared using previously reported methods.[10] Fig. 8C depicts the GIWAXS pattern for a 2D $(C_6H_5C_2H_4NH_3)_2SnI_4$ thin film. The reflection spots located along the q_z axis ($q_{xy} = 0$) at 0.30 and 0.66 A^{-1} are the (001) and (002) crystallographic planes of the $(C_6H_5C_2H_4NH_3)_2SnI_4$ crystal structure, respectively. The GIWAXS pattern presented in Fig. 8C also demonstrates anisotropic intensities around the (001) and (002) crystallographic planes –both being most intense at the meridian ($q_{xy} = 0$). This is an indication that the (00l) planes of $(C_6H_5C_2H_4NH_3)_2SnI_4$ are preferentially oriented parallel to the substrate. Fig. 8D shows the normalized intensity of the (002) reflection of $(C_6H_5C_2H_4NH_3)_2SnI_4$ plotted as a function of azimuthal angle (φ). Based on the azimuthal distribution, we can infer that there is very little spectral noise in the data. We can then proceed to determine MF about the (002) reflection of $(C_6H_5C_2H_4NH_3)_2SnI_4$ assuming $\varphi = 0°$ at the meridian. Accordingly, $MF_{(002)}$ can range from -1 to 1 wherein $MF_{(002)} = 1$ indicates perfect alignment of the crystallites parallel to the substrate; $MF_{(002)} = 0$ indicates no preferential alignment of the crystallites, and -1 indicates orthogonal preferential alignment or in this case in the plane of the substrate. Per equation 8, we obtain $MF_{(002);0°} = 0.93$, indicating that the film is preferentially oriented parallel to the substrate. On the other hand, the HF for the (002) crystallographic plane is 0.22, highlighting how minute amounts of noise within the sample can yield misleading orientation values. As such, the weighted amplitude of a signal applied in MF allows for a less errant orientation value when low levels of noise are present.

Vertically oriented inorganic semiconducting nanowire arrays. Control over the orientation and size of anisotropic one-dimensional (1D) inorganic semiconductors is critical for achieving high performance in many optical and electrical applications. Vertically oriented arrays based on 1D inorganic semiconductors have been demonstrated as unique hierarchical architectures for tuning their physical and electronic properties given the targeted application. In photovoltaics, for example, it can be expected that a device containing 1D nanowire arrays of either zinc oxide (ZnO) or titanium (IV) oxide (TiO_2) will provide direct and ordered paths for the transport of photogenerated electrons as well as a high surface area for light harnessing. In the case of energy storage, using vertically oriented nanowire arrays as active layers would offer the potential for increased power and energy densities

This journal is © The Royal Society of Chemistry 20xx

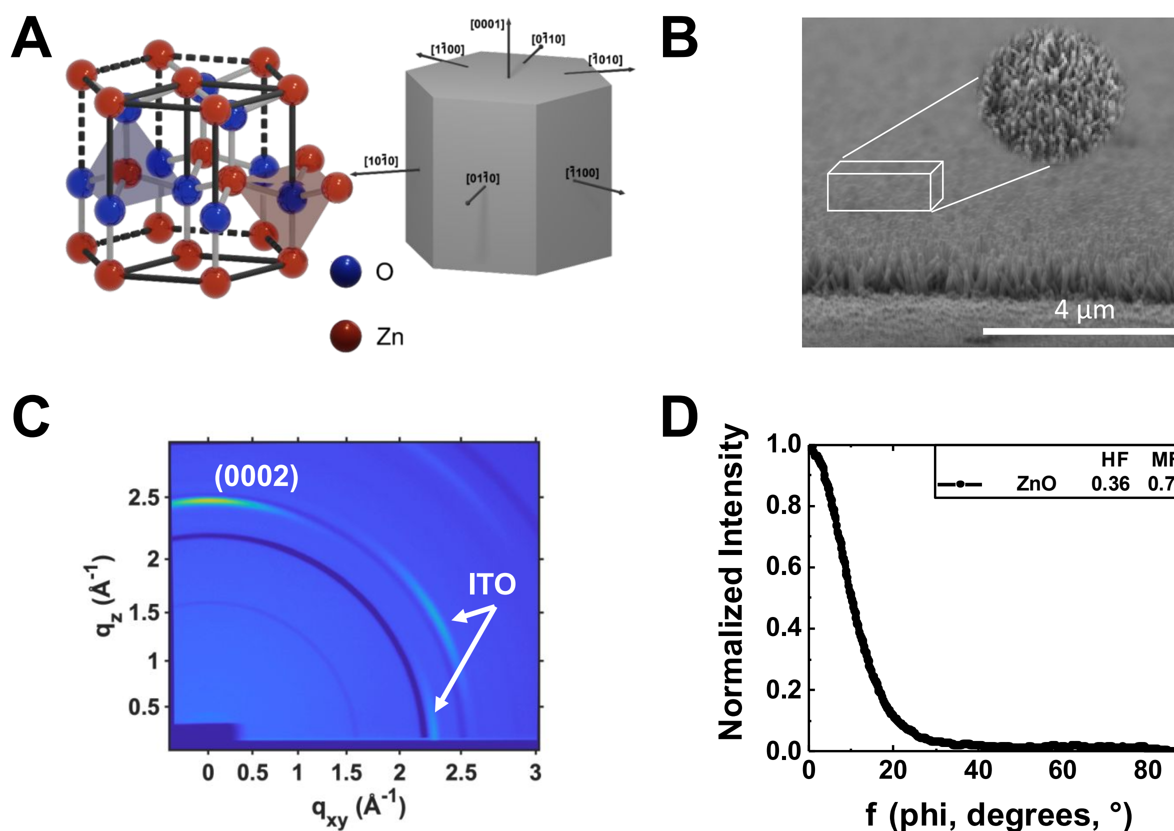

Fig. 9 Case study: zinc oxide nanostructures. (A) 3D representation of the zinc oxide structure with zinc represented with red spheres and oxygen represented by blue spheres. The hexagon reference to the right displays the vectors for each of the Miller indices. (B) Scanning electron micrograph of zinc oxide nanowires with a favorable vertical orientation (C) GIWAXS pattern of a zinc oxide thin film showing structural orientation with the (0002) index reflecting along the out-of-plane direction. (D) Normalized intensity of the (0002) reflection plotted as a function of φ. HF and MF values are also listed.

array and the electrolyte, better control over volume changes upon lithium intercalation/de-intercalation without fracturing, and shorter solid-state diffusion paths. Given that the surface and optoelectronic properties of 1D semiconducting nanowire arrays are predominantly dictated by the anisotropic nature of their crystallites, MF may be instrumental in accurately correlating changes in orientation due to processing conditions to the observed properties. We will focus our attention on ZnO. ZnO nanowire arrays have been widely used in organic light-emitting diodes, transistors, and solar cells, due to their high electron mobility and long electron lifetimes.[18,48–51] As depicted in Fig. 9A, ZnO crystallizes in a hexagonal wurtzite structure where each Zn^{2+} ion is linked to four O^{2-} forming a tetrahedron. The 1D ZnO structure may also be described as being comprised of alternating planes of Zn and O ions stacked along the c-axis (Fig. 9A).[18,51] Fig. 9B shows a cross-sectional scanning electron micrograph of hydrothermally grown ZnO nanowire arrays. Based on the inset, individual nanowires are about 350-nm tall with an average diameter of 50 nm. Fig. 9C depicts an indexed 2D GIWAXS image of a ZnO nanowire array. We observe a very intense reflection at q_z = 2.49 Å^{-1} which corresponds to the (0002) crystallographic plane of the ZnO wurtzite crystal structure. In particular, the (0002) reflection of ZnO is most intense at the meridian (or $q_{xy} = 0$); the (000*l*) planes of ZnO are thus preferentially oriented parallel to the substrate. Given that the fast growth direction of ZnO is along the <0001> direction, the intensity anisotropy of the (0002) reflection is thus also a proxy for the preferential orientation of the nanowires. To quantify the orientation, Fig. 9D illustrates the normalized intensity of the (0002) reflection of ZnO as a function of φ. The $MF_{(0002);0°}$ for this particular crystallographic plane is 0.75, corresponding well to the span in orientation distribution of the ZnO nanowires distributed over a range of ±20° with respect to the substrate normal. Again, due to noise, the HF yields a very low orientation factor of 0.36.

Conductive polymer thin films. Conductive organic polymers such as poly(3,4-ethelynedioxythiophene) -PEDOT have emerged as ideal organic electronic materials exhibiting a widely tunable range of electronic properties and commands interest in polymer science for various thin film applications including thermoelectrics, spintronics, and photovoltaic devices.[52–56] As the electronic properties observed in organic materials are directly associated with the extent of their π conjugation, the orientation in these thin films will play a vital

This journal is © The Royal Society of Chemistry 20xx

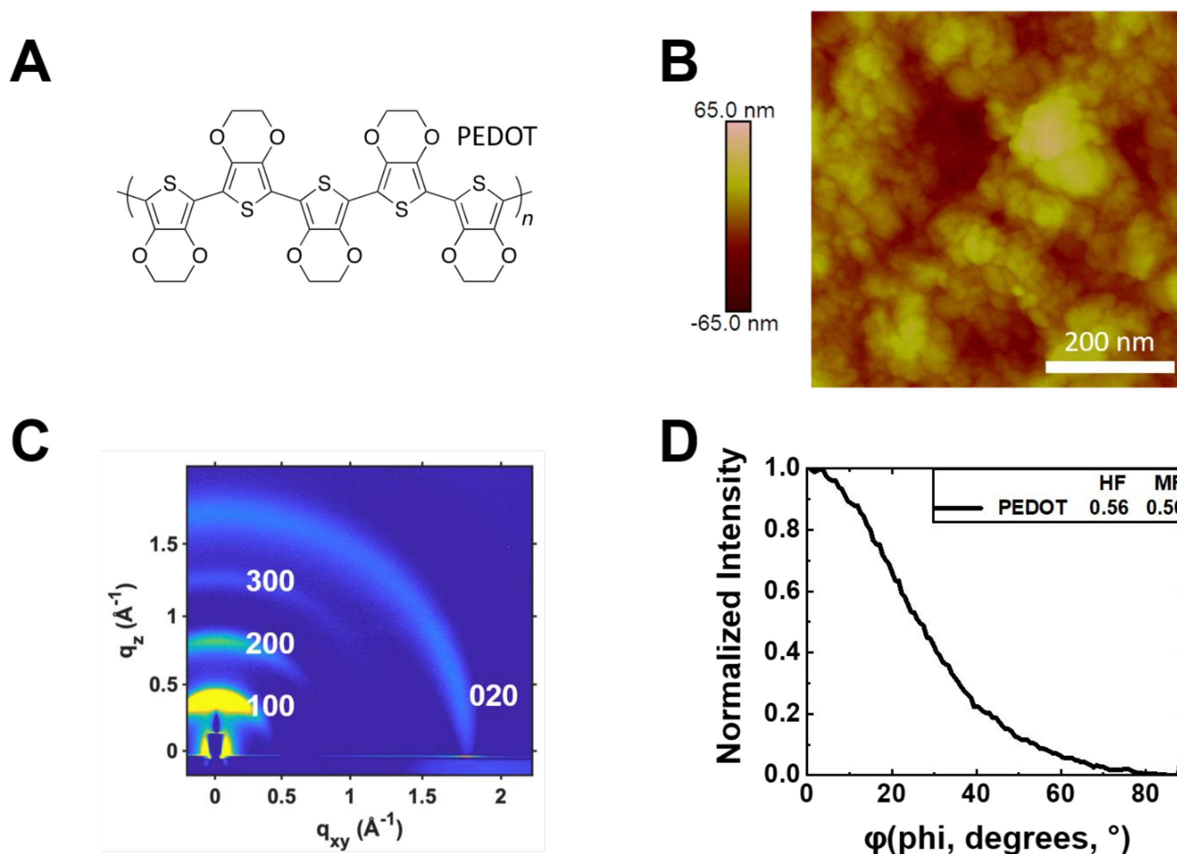

Fig. 10 Case study: PEDOT. (A) The chemical structure for the polymer. (B) Atomic force micrograph of PEDOT showing the morphology, with the roughness listed in the upper right-hand corner. (C) GIWAXS pattern of the PEDOT thin film showing structural orientation with the (l00) indices reflecting along the out-of-plane direction. (D) Normalized intensity of the (200) reflection plotted as a function of φ. HF and MF values are also listed.

role in defining their application. The conjugated polymer PEDOT is no different. A PEDOT molecule consists of interconnected 3,4-ethylenedioxythiophene (EDOT) monomers forming a polymeric backbone (Fig. 10A).[52,57,58] Upon the polymerization of EDOT, a very uniform and continuous PEDOT thin film may be readily assembled on a glass substrate as shown by the atomic force micrograph presented in Fig. 10B. Based on previous works, PEDOT thin films have been shown to transition from an amorphous film to highly crystalline film upon the interaction with certain counterions, such as tosylate.[52,55,56] This is corroborated by the GIWAXS image depicted in Fig. 10C. Here, the reflections observed azimuthally are from the (h00) indices. The orientation of a PEDOT thin film is quantified by using the (200) reflection observed at 0.88 Å^{-1} as shown in Fig. 10D and it is calculated to be $MF_{(200);0^\circ} = 0.56$. This value indicates that crystallites within the PEDOT thin film are oriented out-of-plane with respect to the substrate where (h00) reflections are perpendicular to the π stacking direction. The HF and MF values are the same in the case of the PEDOT thin film. However, a comparison between HF and MF values for the three experimental examples discussed vide supra is telling. Calculation of MF returns orientation values in harmony with a qualitative intuition; both the $(C_6H_5C_2H_4NH_3)_2SnI_4$ and ZnO signal intensity are more narrowly aligned along φ = 0° than the signal observed for PEDOT, and thus sequentially decreasing orientation values from $(C_6H_5C_2H_4NH_3)_2SnI_4$, to ZnO, and PEDOT are expected and observed. Conversely, HF erroneously yields a higher orientation value for PEDOT than for ZnO, which in turn yields a higher orientation than for the $(C_6H_5C_2H_4NH_3)_2SnI_4$ despite the wider Gaussian distribution of the PEDOT signal intensity. This discrepancy is due to the presence of non-zero intensity and noise extending across the entire φ sweep. Using a weighted amplitude for the intensity contribution at every point rather than treating all intensity as equal allows MF to correctly evaluate the orientation for each reflection.

Complex experimental example: the case of 3D OIHP thin films (methylammonium lead iodide, $CH_3NH_3PbI_3$). A significant amount of research attention has been devoted to understanding the morphology and crystallite orientations of $CH_3NH_3PbI_3$ thin films using GIWAXS.[19,59–61] In the most commonly used analog of $CH_3NH_3PbI_3$, the methylammonium cation ($CH_3NH_3^+$) is surrounded by PbI_6 octahedra yielding an overall tetragonal crystal structure (Fig. 11A). Here, we prepared uniform thin films comprising $CH_3NH_3PbI_3$ crystallites via a spin coating process (Fig. 11B).[62] Fig. 11C shows the GIWAXS pattern of a $CH_3NH_3PbI_3$ thin film. The crystallites within the perovskite thin film exhibit a mix of orientations, as can be observed with the (110) reflection at a q spacing of 1.04 Å^{-1}. Fig. 11D shows the intensity of the (110) reflection as a function of φ for a $CH_3NH_3PbI_3$ thin film. This reflection exhibits

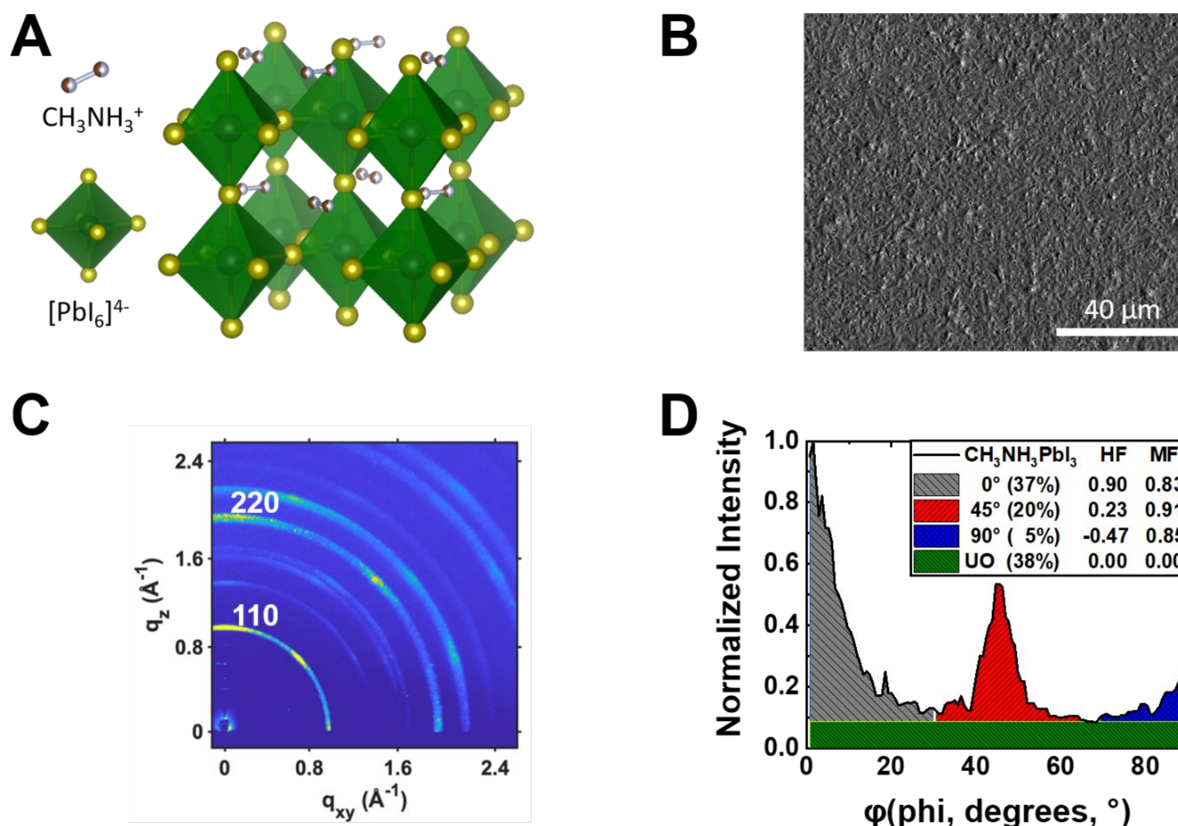

Fig. 11 Case study: methylammonium lead iodide. (A) 3D representation of the methylammonium lead iodide structure comprised of lead iodide octahedra with the ammonium cation coordinated in between the octahedra. (B) Scanning electron micrograph of a methylammonium lead iodide thin film showing a uniform morphology. (C) GIWAXS pattern of a methylammonium lead iodide thin film showing multiple favorable structural orientations with the (110) indices reflecting along both the in and out-of-plane directions and at a 45º angle. (D) Normalized intensity of the (110) reflection plotted as a function of φ. HF and MF values are also listed for clarity. Here, MF quantifies the structural orientation observed along each respective angle, along with the amount of non-oriented (UO) sample present.

crystallites being oriented along 0°, 45°, and 90° as well as crystallites showing no orientation making it an ideal illustrative example for showing how MF can quantify multiple observed orientations within a thin film material. Each component can be quantified as a percentage of the total intensity, where in this case signal oriented along the $MF_{(110);0^o}$ is 37 % of the total diffraction intensity, $MF_{(110);45^o}$ is 20%, $MF_{(110);90^o}$ is 5%, and $MF_{(110);UO}$ (no orientation) is 38% of the total. The orientation of each respective components is then also quantified, showing that $MF_{(110);0^\circ} = 0.83$, $MF_{(110);45^\circ} = 0.91$, $MF_{(110);90^\circ} = 0.85$, and $MF_{(110);UO} = 0$. These results show that $CH_3NH_3PbI_3$ is 37% oriented along the q_z, 20% of the sample is oriented along φ_s = 45°, and only 5% is observed to be oriented along the q_{xy} (φ = 90°) while 38% percent of the sample is not oriented. Of the oriented components, crystallites at 45° with respect to the substrate are more oriented that those at 0° and 90° with respect to the substrate.

Conclusion

We report a new method, the mosaicity factor, or MF, to be used as a tool to compare the orientation of crystallites within a single thin film or between multiple thin films. On its own, an orientation factor has little value but instead is a tool that can be used to study and understand the morphological underpinnings of different thin film technologies. We have thoroughly studied the usefulness of MF in determining the orientation of crystallites within a thin film for both theoretical constructs and experimental data. In all the examples presented, MF can provide detailed information about the orientation of a material. This method is more robust and overcomes limitations that are observed with the previously used method HF. The treatment discussed herein ought not to be misconstrued as an attempt to invalidate past or present use of HF in the literature. MF allows for crystallite orientation to be quantified in all cases where HF is typically used while allowing for enhanced analysis of orientation between systems that typically cannot be quantified using HF. We therefore

 This journal is © The Royal Society of Chemistry 20xx

conclude that MF can and should be used as a tool to quantify crystallite orientation in thin film materials.

Conflicts of interest

There are no conflicts to declare.

Acknowledgments

This work was supported by the AFOSR under Award No. FA9550-18-1-0212. L.W.B. would also like to acknowledge the financial support from the Ovshinsky Sustainable Energy Fellowship administered by the American Physical Society and from the Research Corporation for Science Advancement through a Cottrell Scholar Award. J.O. acknowledges funding from the Utah Governor's Office of Energy Development. GIWAXS studies were conducted at CHESS, which is supported by NSF award # DMR-1332208. We will also like to thank Dr. Anna Hiszpanski and Dr. Rodrigo Noriega for helpful discussions.

References

1 K. Inaba, *Rigaku J.*, 2008, **24**, 10–15.
2 K. Vasseur, K. Broch, A. L. Ayzner, B. P. Rand, D. Cheyns, C. Frank, F. Schreiber, M. F. Toney, L. Froyen and P. Heremans, *ACS Appl. Mater. Interfaces*, 2013, **5**, 8505–8515.
3 J. L. Baker, L. H. Jimison, S. Mannsfeld, S. Volkman, S. Yin, V. Subramanian, A. Salleo, A. P. Alivisatos and M. F. Toney, *Langmuir*, 2010, **26**, 9146–9151.
4 A. M. Hiszpanski, S. S. Lee, H. Wang, A. R. Woll, C. Nuckolls and Y. L. Loo, *ACS Nano*, 2013, **7**, 294–300.
5 N. Tanigaki, T. Mizokuro, T. Miyadera, Y. Shibata and T. Koganezawa, *Jpn. J. Appl. Phys.*, 2018, **57**, 1–6.
6 K. Mukai, *J. Nanoelectron. Optoelectron.*, 2018, **7**, 245–254.
7 D. W. Breiby, O. Bunk, J. W. Andreasen, H. T. Lemke and M. M. Nielsen, *J. Appl. Crystallogr.*, 2008, **41**, 262–271.
8 A. S. M. Tripathi, M. Pandey, S. Sadakata, S. Nagamatsu, W. Takashima, S. Hayase and S. S. Pandy, *Appl. Phys. Lett.*, 2018, **112**, 1–5.
9 N. Boulanger, V. Yu, M. Hilke, M. F. Toney and D. R. Barbero, *Phys. Chem. Chem. Phys.*, 2017, **19**, 8496–8503.
10 E. Amerling, S. Baniya, E. Lafalce, C. Zhang, Z. V. Vardeny and L. Whittaker-brooks, *J. Phys. Chem. Lett.*, 2017, **8**, 4557–4564.
11 M. F. Toney, D. Nordlund, J. H. Oh, Y. Sun and W. Frank, *Chem. Mater.*, 2009, **21**, 5508–5518.
12 H. Lee, J. S. Lee, S. Cho, H. Kim, K. Kwak, Y. Yoon, S. K. Son, H. Kim, M. J. Ko, D. Lee, J. Y. Kim, S. Park, D. H. Choi, S. Y. Oh, J. H. Cho and B. Kim, *J. Phys. Chem. C*, 2012, **116**, 26204–26213.
13 A. Tixier-mita, S. Ihida, B. Ségard, G. A. Cathcart, T. Takahashi, H. Fujita and H. Toshiyoshi, *Jpn. J. Appl. Phys.*, 2016, **55**, 1–9.
14 J. Sheng, H. Jeong, K. Han, T. Hong and J. Park, *J. Inf. Disp.*, 2017, **18**, 159–172.
15 S. Sohn, K. H. Park, S. Kwon, H. Lee, H. Ahn, S. Jung and Y. Kim, *ACS Omega*, 2018, **3**, 9989–9996.
16 X. Liu, L. Nian, K. Gao, L. Zhang, L. Qing, Z. Wang, L. Ying, Z. Xie, Y. Ma, Y. Cao, F. Liu and J. Chen, *J. Mater. Chem. A*, 2017, **5**, 17619–17631.
17 T. D. Lee, A. Ebong and S. M. Ieee, *IEEE*, 2015, **15**, 33–42.
18 L. Whittaker-Brooks, W. E. McClain, J. Schwartz and Y. L. Loo, *Adv. Energy Mater.*, 2014, **4**, 1–7.
19 W. J. Nimens, J. Ogle, A. Caruso, M. Jonely, C. Simon, D. Smilgies, R. Noriega, M. Scarpulla and L. Whittaker-Brooks, *ACS Appl. Energy Mater.*, 2018, **1**, 602–615.
20 A. Degrauw, R. Armstrong, A. A. Rahman, J. Ogle and L. Whittaker-Brooks, *Mater. Res. Express*, 2017, **4**, 1–10.
21 Y. Zhou, X. Han, X. Hu and L. Xu, *High Perform. Polym.*, 2017, **29**, 1158–1164.
22 D. Liu, X. Li, H. Song, P. Wang, J. Chen, Q. Tian, L. Sun, L. Chen, B. Chen, J. Gong and G. Sun, *Eur. Polym. J.*, 2018, **99**, 18–26.
23 Y. Mao, M. Bleuel, Y. Lyu, X. Zhang, D. Henderson, H. Wang and R. M. Briber, *Langmuir*, 2018, **34**, 8042–8051.
24 J. J. Hermans, P. H. Hermans, D. Vermaas and A. Weidinger, *Recl. des Trav. Chim. des Pays-Bas*, 1946, **65**, 427–447.
25 G. R. Strobl, *The Physics of Polymers*, Springer, Berlin, 3rd edn., 2007.
26 D. Campbell, R. A. Pethrick and J. R. White, *Polymer Characterization*, Stanley Thornes Ltd, Cheltenham, 2nd edn., 2000.
27 P. H. Hermans and A. Weidinger, *J. Appl. Phys.*, 1948, **19**, 491–506.
28 Z. Jiang, *J. Appl. Crystallogr.*, 2015, **48**, 917–926.
29 N. Widjonarko, *Coatings*, 2016, **6**, 54–71.
30 D. M. Smilgies, D. R. Blasini, S. Hotta and H. Yanagi, *J. Synchrotron Radiat.*, 2005, **12**, 807–811.
31 D.-M. Smilgies and D. R. Blasini, *J. Appl. Crystallogr.*, 2007, **40**, 716–718.
32 D.-M. Smilgies, *J. Appl. Crystallogr.*, 2009, **42**, 1030–1034.
33 M. B. Johnston and L. M. Herz, *Acc. Chem. Res.*, 2016, **49**, 146–154.
34 Y. Zhao and K. Zhu, *Chem. Soc. Rev.*, 2016, **45**, 655–689.
35 C. C. Stoumpos, D. H. Cao, D. J. Clark, J. Young, J. M. Rondinelli, J. I. Jang, J. T. Hupp and M. G. Kanatzidis, *Chem. Mater.*, 2016, **28**, 2852–2867.
36 H. Tsai, W. Nie, J.-C. Blancon, C. C. Stoumpos, R. Asadpour, B. Harutyunyan, A. J. Neukirch, R. Verduzco, J. J. Crochet, S. Tretiak, L. Pedesseau, J. Even, M. A. Alam, G. Gupta, J. Lou, P. M. Ajayan, M. J. Bedzyk, M. G. Kanatzidis and A. D. Mohite, *Nature*, 2016, **536**, 312–316.
37 J. Peng, Y. Chen, K. Zheng, T. Pullerits and Z. Liang, *Chem. Soc. Rev.*, 2017, **46**, 5714–5729.
38 B. Zhao, S. Bai, V. Kim, R. Lamboll, R. Shivanna, F. Auras, J. M. Richter, L. Yang, L. Dai, M. Alsari, X. J. She, L. Liang, J. Zhang, S. Lilliu, P. Gao, H. J. Snaith, J. Wang, N. C. Greenham, R. H. Friend and D. Di, *Nat. Photonics*, 2018, **12**, 783–789.
39 M. Wei, W. Sun, Y. Liu, Z. Liu, L. Xiao, Z. Bian and Z. Chen, *Phys. Status Solidi Appl. Mater. Sci.*, 2016, **213**, 2727–2732.
40 Q. Chen, N. De Marco, Y. (Michael) Yang, T.-B. Song, C.-C.

Chen, H. Zhao, Z. Hong, H. Zhou and Y. Yang, *Nano Today*, 2015, **10**, 355–396.
41 C. C. Boyd, R. Cheacharoen, T. Leijtens and M. D. McGehee, *Chem. Rev.*, 2019, **119**, 3418–3451.
42 M. Alsari, A. J. Pearson, J. T. W. Wang, Z. Wang, A. Montisci, N. C. Greenham, H. J. Snaith, S. Lilliu and R. H. Friend, *Sci. Rep.*, 2018, **8**, 1–6.
43 G. P. Nagabhushana, R. Shivaramaiah and A. Navrotsky, *Proc. Natl. Acad. Sci.*, 2016, **113**, 7717–7721.
44 A. Buin, R. Comin, J. Xu, A. H. Ip and E. H. Sargent, *Chem. Mater.*, 2015, **27**, 4405–4412.
45 J. Lee, J. Ruff, M. Yoon, J. J. Choi and S. Lee, *Sci. Adv.*, 2016, **2**, 1–14.
46 J. V. Passarelli, D. J. Fairfield, N. A. Sather, M. P. Hendricks, H. Sai, C. L. Stern and S. I. Stupp, *J. Am. Chem. Soc.*, 2018, **140**, 7313–7323.
47 J. Jagielski, S. Kumar, W. Y. Yu and C. J. Shih, *J. Mater. Chem. C*, 2017, **5**, 5610–5627.
48 B. Y. Oh, Y. H. Kim, H. J. Lee, B. Y. Kim, H. G. Park, J. W. Han, G. S. Heo, T. W. Kim, K. Y. Kim and D. S. Seo, *Semicond. Sci. Technol.*, 2011, **26**, 1–5.
49 J. Huang, Z. Yin and Q. Zheng, *Energy Environ. Sci.*, 2011, **4**, 3861–3877.
50 K. M. Sandeep, S. Bhat and S. M. Dharmaprakash, *J. Phys. Chem. Solids*, 2017, **104**, 36–44.
51 L. Whittaker-Brooks, J. M. Mativetsky, A. Woll, D. Smilgies and Y. L. Loo, *Org. Electron. physics, Mater. Appl.*, 2013, **14**, 3477–3483.
52 O. Bubnova, Z. U. Khan, H. Wang, S. Braun, D. R. Evans, M. Fabretto, P. Hojati-Talemi, D. Dagnelund, J. B. Arlin, Y. H. Geerts, S. Desbief, D. W. Breiby, J. W. Andreasen, R. Lazzaroni, W. M. Chen, I. Zozoulenko, M. Fahlman, P. J. Murphy, M. Berggren and X. Crispin, *Nat. Mater.*, 2014, **13**, 190–194.
53 S. J. Lee, H. Pil Kim, A. R. Bin Mohd Yusoff and J. Jang, *Sol. Energy Mater. Sol. Cells*, 2014, **120**, 238–243.
54 T. V. A. G. De Oliveira, M. Gobbi, J. M. Porro, L. E. Hueso and A. M. Bittner, *Nanotechnology*, 2013, **24**, 1–10.
55 Z. U. Khan, O. Bubnova, M. J. Jafari, R. Brooke, X. Liu, R. Gabrielsson, T. Ederth, D. R. Evans, J. W. Andreasen, M. Fahlman and X. Crispin, *J. Mater. Chem. C*, 2015, **3**, 10616–10623.
56 I. Petsagkourakis, E. Pavlopoulou, G. Portale, B. A. Kuropatwa, S. Dilhaire, G. Fleury and G. Hadziioannou, *Sci. Rep.*, 2016, **6**, 1–8.
57 X. Crispin, S. Marciniak, W. Osikowicz, G. Zotti, a W. D. V. a N. D. E. R. Gon, F. Louwet, M. Fahlman, L. Groenendaal, F. D. E. Schryver and W. R. Salaneck, *Polymer (Guildf).*, 2003, **41**, 2561–2583.
58 T. Park, C. Park, B. Kim, H. Shin and E. Kim, *Energy Environ. Sci.*, 2013, **6**, 788–792.
59 N.-K. Kim, Y. H. Min, S. Noh, E. Cho, G. Jeong, M. Joo, S.-W. Ahn, J. S. Lee, S. Kim, K. Ihm, H. Ahn, Y. Kang, H.-S. Lee and D. Kim, *Sci. Rep.*, 2017, **7**, 1–9.
60 B. J. Foley, J. Girard, B. A. Sorenson, A. Z. Chen, J. Scott Niezgoda, M. R. Alpert, A. F. Harper, D. M. Smilgies, P. Clancy, W. A. Saidi and J. J. Choi, *J. Mater. Chem. A*, 2017, **5**, 113–123.
61 Y. Tidhar, E. Edri, H. Weissman, D. Zohar, G. Hodes, D. Cahen, B. Rybtchinski and S. Kirmayer, *J. Am. Chem. Soc.*, 2014, **136**, 13249–13256.
62 W. J. Nimens, S. J. Lefave, L. Flannery, J. Ogle, D. M. Smilgies, M. T. Kieber-Emmons and L. Whittaker-Brooks, *Angew. Chem. Int. Ed.*, 2019, DOI:10.1002/anie.201906017.

 This journal is © The Royal Society of Chemistry 20xx

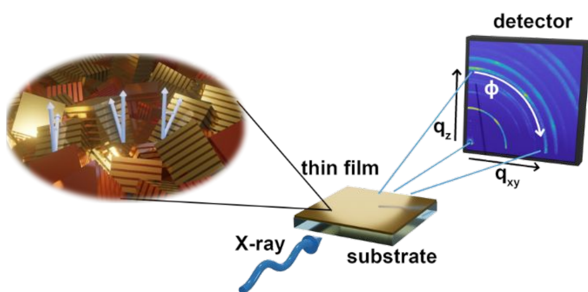

Using the mosaicity factor and GIWAXS diffraction patterns to quantify crystallite heterogeneities and orientation in thin film materials